JOURNAL OF GEOPHYSICAL RESEARCH: ATMOSPHERES, VOL. 118, 467–480, doi:10.1029/2012JD018323, 2013

Increased summer rainfall in northwest Australia linked to southern Indian Ocean climate variability

Juan Feng,[1] Jianping Li,[1] and Hanlie Xu[1]

Received 19 June 2012; revised 31 October 2012; accepted 1 November 2012; published 30 January 2013.

[1] Although annual rainfall over most of Australia has followed a continuously decreasing trend over the past 6 decades (i.e., 1948–2007), summer rainfall in northwest Australia (NWA) has followed a pronounced increasing trend, with a significant linear trend of 2.65 mm/yr. This study investigates the causes of increasing rainfall over NWA and focuses on influences originating in the middle to high latitudes, i.e., southern Indian Ocean climate variability. Our results indicate that variations in summer rainfall over NWA are related to the concurrent strength of the Mascarene high. In years with a strong Mascarene high in the lower troposphere, the cyclonic vorticity over NWA is enhanced, and more moisture is transported into NWA. Simultaneously, an anomalous vertical closed circulation forms, with an ascending branch over NWA and subsidence over the region occupied by the Mascarene high. As for the upper troposphere, the Mascarene high is related to a teleconnection wave train from the southern Indian Ocean to NWA, which in turn influences the circulation over NWA. This setting is favorable for enhanced rainfall over NWA. Analysis of the cause of variations in the Mascarene high indicates that underlying external forcing of the high by, for example, sea surface temperature (SST) has intensified, possibly due to the influence of the southern annular mode (SAM) during the preceding spring. This mechanism was further examined using numerical experiments. We believe that the strengthening of the Mascarene high, which is caused by the enhanced SST gradient within the southern Indian Ocean associated with the preceding (upward) SAM, has had a significant influence on the increase in summer rainfall over NWA.

Citation: Feng J., J. Li, and H. Xu (2013), Increased summer rainfall in northwest Australia linked to southern Indian Ocean climate variability, *J. Geophys. Res. Atmos., 118*, 467–480, doi:10.1029/2012JD018323.

1. Introduction

[2] Rainfall in Australia is highly variable, both spatially and temporally [*Drosdowsky*, 1993; *Murphy and Ribbe*, 2004], and this has important implications for both agriculture and the management of water resources. Consequently, an improved understanding of the causes of precipitation variability would assist future investigations of the climatic variations, and is necessary to minimize weather-related financial losses. Since the middle of the 20th century, the observed austral summer rainfall (December–February, DJF) in northwest Australia (NWA) has increased by about 50% of its climatological value [*Smith*, 2004]. In contrast, this period has seen a continuous decreasing trend in rainfall during the rainy season in southwest Western Australia (bounded by a line between 30°S, 115°E and 35°S, 120°E), which receives the bulk of its annual rainfall between June and August [e.g., *Smith et al*., 2000; *Indian Ocean Climate Initiative*, 2002; *Feng et al*., 2010a], in northeast Australia (eastward of 140°E and northward of 25°S), which receives the bulk of its annual rainfall from December to February [e.g., *Taschetto and England*, 2008; *Li et al*., 2012], and southeast Australia, which includes the Murray-Darling Basin and the southeast coast drainage divisions, which receives the bulk of its annual rainfall from June to August). Therefore, a long-term increase in rainfall over NWA would represent an important element in the water management strategy for the region.

[3] The distinct regional characteristics of rainfall variability in Australia highlight the diverse range of climatic drivers that influence rainfall throughout the continent. The potential impacts of climatic modes within the tropics, such as the El Niño–Southern Oscillation (ENSO), Indian Ocean dipole (IOD) [*Saji et al*., 1999], and ENSO Modoki (EM) [*Ashok et al*., 2007] have been extensively examined. Previous studies have demonstrated that warm El Niño events are generally accompanied by drought conditions over northern and eastern Australia, whereas above-average rainfall occurs in these regions during La Niña events [e.g., *McBride and Nicholls*, 1983; *Drosdowsky and Williams*, 1991; *Wang and Hendon*, 2007]. Recent studies have examined the influence of Indian Ocean sea surface temperature (SST) anomalies on Australian rainfall. For

[1]State Key Laboratory of Numerical Modeling for Atmospheric Sciences and Geophysical Fluid Dynamics, Institute of Atmospheric Physics, Chinese Academy of Sciences, Beijing, China.

Corresponding author: J. Li, State Key Laboratory of Numerical Modeling for Atmospheric Sciences and Geophysical Fluid Dynamics, Institute of Atmospheric Physics, Chinese Academy of Sciences, P.O. Box 9804, Beijing 100029, China. (ljp@lasg.iap.ac.cn)

2169-897X/13/2012JD018323

example, *Nicholls et al*. [1996] reported an apparent change in the relationship between ENSO and Australian rainfall and temperature that was caused by an increase in Indian Ocean SST. Subsequently, *Ashok et al*. [2003] and *England et al*. [2006] studied the seasonal influence of the IOD on Australian rainfall. More recent studies have shown that ENSO and EM have contrasting impacts on regional climate [e.g., *Weng et al*., 2007; *Feng and Li*, 2011; *Zhang et al*., 2011]. Accordingly, the influence of EM on Australian rainfall has been explored [e.g., *Taschetto and England*, 2009; *Weng et al*., 2009], revealing that the influence of EM on the regional Australian climate differs to that of ENSO.

[4] The tropical Australian summer monsoon (TASM), which is the southern component of the prominent monsoon systems of Asia and Australia, has a significant influence on rainfall over Australia [*Hung and Yanai*, 2004]. *Li et al*. [2012] pointed out that the weakening of the TASM has contributed to a decrease in summer rainfall over northeast Australia within period 1948–2007. In terms of the extratropics, previous studies have explored the influence of the southern annular mode (SAM) on rainfall [e.g., *Li et al*., 2005; *Wheeler*, 2008; *Feng et al*., 2010b] and temperature [e.g., *Hendon et al*., 2007] in Australia. These studies suggest that rainfall variability in Australia is complex, and controlled by multiple climatic systems with both tropical and extratropical origins.

[5] The mean linear trend in summer (DJF) rainfall for Australia between 1948 and 2007 shows that the largest positive value occurs across much of NWA, with a maximum located several hundred kilometers inland from the coast (Figure 1b). Several different explanations have been provided for this trend. *Wardle and Smith* [2004] simulated an increase in NWA summer rainfall by reducing the surface albedo over the continent; however, their prescribed decreases in albedo were much larger than the actual decreases. *Rotstayn et al*. [2007] reported that including (excluding) anthropogenic aerosol changes during the 20th century generates increasing (decreasing) rainfall over Australia; however, as they indicated, there are a number of limitations associated with their results, including the simplified and uncertain treatment of aerosol processes. Subsequently, *Shi et al*. [2008] suggested that the increase is due to a westward shift in the ENSO-related rainfall variability from the northeast toward NWA. In addition, other work indicates that changes to the onset of the Australian monsoon [*Taschetto and England*, 2008] and

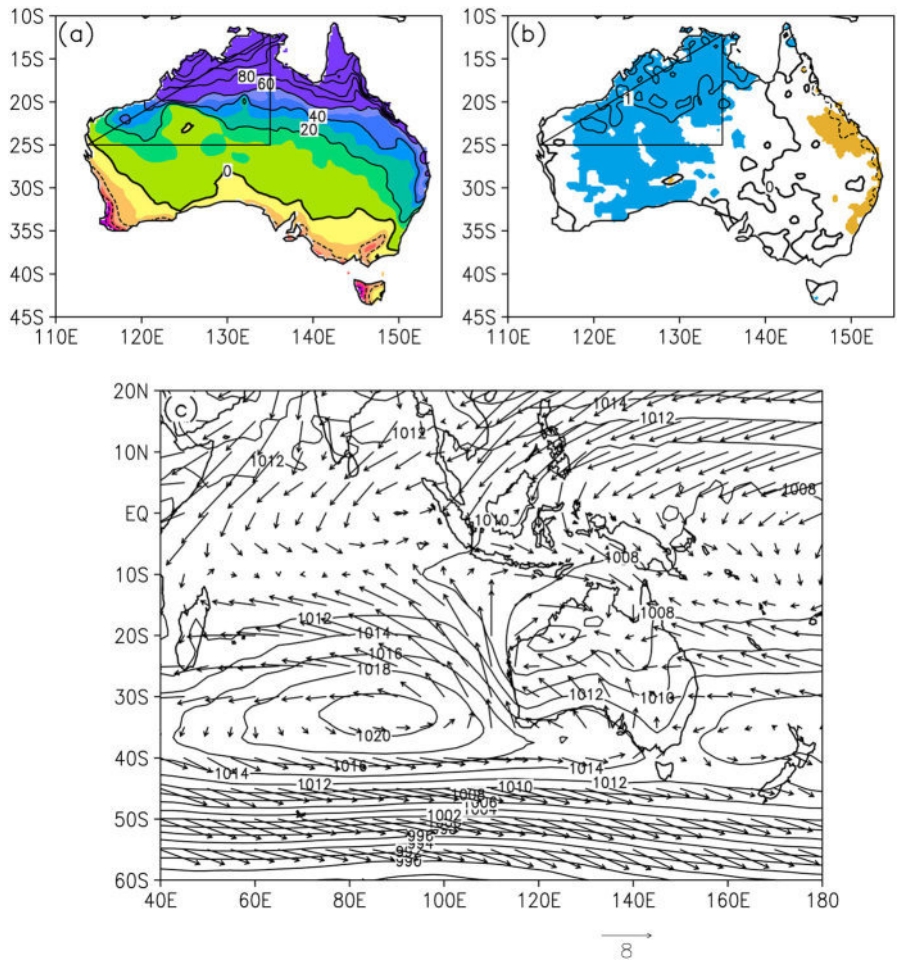

Figure 1. (a) Climatological summer (DJF) rainfall departure from the annual mean (mm/month). (b) Summer rainfall trend (mm/yr). (c) Circulation at 925 hPa, with contours for sea level pressure (hPa) and vectors for winds at 925 hPa (m/s). We define northwest Australia as the area west of 135°E and north of 25°S, as shown in Figures 1a and 1b. Shading in Figure 1b indicates significance at the 0.05 level.

synoptic weather systems [*Berry et al*., 2011] also contribute to an increase in NWA summer rainfall.

[6] While these previous studies have improved our understanding of the nature and causes of variations in NWA summer rainfall, they have not been able to explain the recorded rainfall variations. In addition, most have focused on influences from the tropics, rather than from the extratropics, e.g., the southern Indian Ocean. Very recently, *Lin and Li* [2012] have shown that an increasing trend in atmospheric ascent induced by a warming SST trend in the tropical Atlantic may partially explain the increased rainfall in NWA. They suggest that the teleconnection is via the south Indian Ocean, but they did not illustrate how the signal transfers from the south Indian Ocean to NWA. In fact, the variability in the southern Indian Ocean, and its relationship with other climate features, has received recent interest [*Terray et al*., 2005; *Yoo et al*., 2006]. As mentioned above, many studies have already shown that extratropical climate systems may influence tropical regions [*Thompson and Lorenz*, 2004; *Wu et al*., 2009a, 2009b, 2012; *Zheng and Li*, 2012]. However, there has been little discussion of the impacts of extratropical climate systems on summer rainfall variations in NWA. Therefore, it is important to consider whether extratropical climate systems contribute to variations in summer rainfall over NWA, as well as the relevant physical processes and plausible mechanisms. A better understanding of these issues would assist future investigations of rainfall variations in NWA.

[7] The above considerations provide the motivation for the present study. Our findings show that variations in NWA summer rainfall are closely linked to variability in extratropical climate systems. The remainder of this paper is organized as follows. The data sets and methods are described in section 2, and the circulation anomalies associated with NWA summer rainfall are presented in section 3. In section 4, we examine the relationship between the Mascarene high and NWA summer rainfall, and section 5 considers the physical mechanism that underlies this relationship. Finally, a brief summary and conclusions are presented in section 6.

2. Data, Methods, and Model

[8] This study used high-resolution (0.25° latitude-longitude) gridded rainfall data provided by the Australian Bureau of Meteorology for the period between 1948 and 2007, which were superseded by a set of 3D topography-resolving analyses [*Jones and Weymouth*, 1997]. Atmospheric fields were obtained from the National Centers for Environmental Prediction/National Center for Atmospheric Research (NCEP/NCAR) reanalysis [*Kalnay et al*., 1996]. SST data were the improved extended reconstruction SST (IERSST) on a 2° × 2° grid [*Smith and Reynolds*, 2004]. The SAM index (SAMI) used here was defined as the difference in the normalized monthly zonal mean sea level pressure (SLP) between 40°S and 70°S [*Nan and Li*, 2003; http://ljp.lasg.ac.cn/dct/page/65572], and was based on the NCEP/NCAR reanalysis data. Note that the SAMI used here is strongly correlated with the SAM index, defined as the leading empirical orthogonal function (EOF) of SLP anomalies south of 20°S [*Thompson and Wallace*, 2000], yielding a correlation coefficient of 0.96 for the period 1948–2007. Thus, the SAMI used in the present study is appropriate in terms of capturing the features of SAM. The Niño 3.4 index used for canonical ENSO phenomena is available online (at http://www.cpc.ncep.noaa.gov/data/indices/), and the IOD index (IODI) was defined according to the method of *Saji et al*. [1999]. The data sets used in this study cover a period of 60 years from 1948 to 2007, and the DJF value for 1948 refers to the average value for December 1948 and January and February 1949.

[9] Correlation and composite analysis were used to determine the relationship between the Mascarene high and NWA summer rainfall. In particular, the partial correlation method [e.g., *Ashok et al*., 2003], which is often used to describe the relationship between two variables when the effects of another variable have been removed, was introduced to describe the relationship between the Mascarene high and rainfall after removing the effects of other large-scale systems such as the ENSO and IOD.

[10] The atmospheric general circulation model used in this study was the NCAR Community Atmospheric Model version 3.1 (CAM3) [*Collins et al*., 2006]. The CAM is the latest in a series of global atmospheric models developed at NCAR for the weather and climate research communities. CAM also serves as the atmospheric component of the Community Climate System Model (CCSM). The horizontal resolution is T42 (approximately 2.8° latitude × 2.8° longitude), with 26 hybrid vertical levels (for a detailed description of this version of the model, see http://www.ccsm.ucar.edu/models/atm-cam/docs/description/).

3. Circulation Anomalies Associated With NWA Summer Rainfall

[11] Figure 1 shows the normal summer climate fields for reference, and also to demonstrate the background setting and illustrate the differences between wet and dry summers in NWA. Figure 1a shows the climatology of the distribution of summer rainfall in Australia, after subtracting the annual mean for the period 1948–2006. A positive departure is seen north of 25°S, with the maximum value located along the northern coast. From north to south, there is a rapid decrease in rainfall over NWA. Regarding the circulation (Figure 1c), the Australian low is centered over NWA at around 130°E, 18°S. Thus, NWA is controlled by a cyclonic circulation with southerlies prevailing along the western coastal region, westerlies over the northern coast, and easterlies over inland areas. To the south, the Mascarene high lies over the southern Indian Ocean, centered around 90°E, 35°S, and extending as far north as 20°S. Consequently, southerlies prevail along the coast of Western Australia, which corresponds to the western edge of the Australian low. This configuration raises the possibility that the Mascarene high acts to influence the strength of the Australian low, which in turn affects rainfall over NWA.

[12] To provide some insight into rainfall variations associated with this pattern of circulation, we investigated spatial changes in lower tropospheric flow in the Australian region by analyzing composite difference maps of wind and geopotential height at 925 hPa for wet-minus-dry summers in NWA (Figure 2). The wet and dry years selected were the eight maximum and eight minimum years of NWA summer rainfall; the wet years are 1973, 1981, 1996, 1998, 1999, 2000, 2003, and 2005, while the dry years are 1951, 1952,

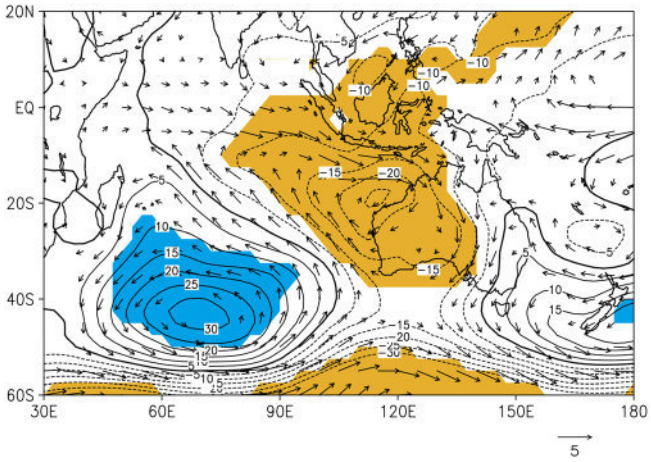

Figure 2. Composite differences in geopotential height (contours; geopotential meters) and winds (vectors; m/s) at 925 hPa between years with wet and dry summers in northwest Australia. The wind vectors shown are those significant at the 0.05 level. Shading indicates geopotential height anomalies significant at the 0.05 level. The wet years are 1973, 1981, 1996, 1998, 1999, 2000, 2003, and 2005, while the dry years are 1951, 1952, 1953, 1963, 1964, 1969, 1982, and 1991.

1953, 1963, 1964, 1969, 1982, and 1991. Note that if a definition that normalized values beyond/below one positive/negative standard deviation was employed, there would have been 8 dry years and 12 wet years. In this case, the sample size for the wet years would be 1.5 times greater than that for the dry years. Consequently, we took the eight wettest years and eight driest years as the sample to perform the composite analysis. The wet and dry NWA summers have the opposite sign and equivalent magnitude (figure not shown), indicating that the processes leading to an increase in NWA summer rainfall are similar to those that cause its rainfall to decrease. Therefore, in the following discussion, we refer to the wet-minus-dry composite differences as anomalous conditions during the wet summers in NWA. Here, the composite map of wet-minus-dry summers corresponds to conditions associated with a change in the NWA summer rainfall time series (defined as the area-averaged summer rainfall over NWA) of approximately two standard deviations.

[13] There are distinct differences in lower tropospheric circulation between wet and dry NWA summers. Positive anomalies in geopotential height are seen over the southern Indian Ocean, indicating that the Mascarene high would be intensified during wet NWA summers, which is consistent with Figure 17 in *Shi et al*. [2008], despite different regions being the focus (i.e., they concentrated on influences from the tropics). It is notable that the center of the anomalous positive geopotential height of the Mascarene high is not superimposed on its position in the climatology, but has shifted to the south. This is because (1) the southern part of the Mascarene high shows larger variance (i.e., south of 40°S; figure not shown), (2) the ridge of the Mascarene high would shift southward in wet NWA years compared with dry years (figure not shown), and (3) the ridge of the Mascarene high would shift southward in the strong Mascarene high years compared with weak years. That is, the southward shift is a reflection of the enhancement of the Mascarene high, and this interpretation is supported by the high correlation between the strength of the Mascarene high (MHI; defined as the SLP averaged over the region 60°–100°E, 40°–30°S) and its ridge position (correlation coefficient of –0.60). Accordingly, the anticyclonic circulation is strengthened, with strong southeasterlies over the ocean west of NWA, resulting in enhanced cyclonic vorticity over NWA and the adjacent ocean to the west. This finding is supported by the strong correlations (Table 1) between NWA summer rainfall and the zonal shear of the meridional wind index (V_{shear}; R = 0.80) and the strength of the Australian low (ALI; R = –0.88). We define V_{shear} as the difference in the meridional wind at 925 hPa between the regions (95°–105°E, 35°–25°S) and (130°–140°E, 20°–10°S); this definition is not dependent on the level selected, and a similar result is seen if 850 hPa is used. ALI is defined as the area-averaged vorticity over 110°–130°E, 25°–15°S at 850 hPa, but because the geopotential height field becomes ambiguous in the low latitudes [*Hsu and Lin*, 1992] the vorticity field is employed to define the strength of the Australian low, as recommended by *Grose and Hoskins* [1979]. Note that the detrended correlations between these parameters are relatively constant (Table 1), and the relationship is significant during the period 1979–2007 when the NCEP/NCAR reanalyses are believed to be more reliable, confirming the connections among variations of the NWA summer rainfall, Australian low, and zonal shear of the meridional wind at an interannual timescale. Furthermore, given the significant trend in NWA summer rainfall, and noting that most of the wet years occur after 1975, to avoid the possible influence of the linear trend the composite differences were further examined after first removing this linear trend (figure not shown). To be pointed out is that if the detrended rainfall is employed to define the wet and dry years, the cases for the composite would have some differences; however, we found a similar anomalous pattern to that shown in Figure 2, implying that the anomalous

Table 1. Raw and Detrended Correlation Coefficients Among Different Indices for 1948–2007 and 1979–2007[a]

	MHI	V_{shear} Index	IATI	Rainfall
Rainfall	**0.48** (**0.40**) [**0.46**]	**0.80** (**0.71**) [**0.79**]	**0.64** (**0.51**) [**0.66**]	
ALI	**–0.43** (**–0.33**) [**–0.44**]	**–0.80** (**–0.77**) [**–0.78**]	**–0.63** (**–0.53**) [**–0.62**]	**–0.88** (**–0.86**) [**–0.86**]
SIOSGI	**0.62** (**0.56**) [**0.62**]	**0.37** (0.26) [**0.51**]	**0.61** (**0.52**) [**0.57**]	**0.38** (0.25) [**0.38**]

[a]The detrended correlation coefficients are given in parentheses, and those for 1979–2007 are given in brackets. Correlation coefficients significant at the 0.05 level are in bold. MHI is defined as the area-averaged SLP over the region 60°–100°E, 40°–30°S. The V_{shear} index is defined as the difference in meridional wind at 925 hPa between the regions 95°–105°E, 35°–25°S and 130°–140°E, 20°–10°S. (3) IATI is defined as the sum of the vorticity at 200 hPa, IAT = A (80°E, 45°S) – B (90°E, 32.5°S) + C (115°E, 25°S) – D (130°E, 15°S). ALI is defined as the area-averaged vorticity over 110°–130°E, 25°–15°S at 850 hPa. SIOSGI is defined as the difference in SST anomalies between the regions 40°–80°E, 44°–34°S and 80°–120°E, 62°–52°S.

circulation is not due to the linear trend. Thus, a significant negative SLP anomaly lies over NWA and the adjacent ocean. This pattern acts to intensify the Australian low located over NWA during the summertime (Figure 1c), and NWA is covered by an anomalous pattern comprising a strong cyclonic circulation. The strengthened cyclonic vorticity is accompanied by enhanced rainfall over NWA. Moreover, the MHI is closely linked to NWA summer rainfall (correlation coefficient of 0.48, significant at the 0.01 level), suggesting that temporal variability in NWA summer rainfall is related to variations in the Mascarene high. In the following section, we consider the degree to which the Mascarene high influences NWA summer rainfall.

4. Relationship Between the Mascarene High and NWA Summer Rainfall

[14] In the previous section, we showed that variations in summer rainfall over NWA are closely linked to the strength of the Mascarene high. To further illustrate the relationship between the Mascarene high and summer rainfall over NWA, the spatial distribution of correlation between the MHI and Australian summer rainfall is shown in Figure 3 and indicates a positive correlation over the NWA region. Hence, the Mascarene high has a positive influence on NWA summer rainfall. Moreover, to determine the impacts of the ENSO and IOD on the Mascarene high–NWA summer rainfall relationship, we calculated the partial correlations between the MHI and rainfall after removing the effect of the ENSO and IOD (Figures 3b and 3c). Our results show that there is little change in the Mascarene high–NWA summer rainfall relationship when their effects are removed from the Mascarene high and rainfall. This suggests that the Mascarene high–NWA summer rainfall relationship is linearly independent from the impact of the ENSO and IOD.

[15] This observation leads to the following question: What is the physical process that connects the influence of the Mascarene high to NWA summer rainfall? To investigate their dynamical linkages, Figure 4 shows the composite differences between the strong and weak Mascarene high years in terms of winds and divergence in the lower troposphere, vertically integrated moisture transport, the zonal mean of vertical velocity, and meridional wind, and reveals significant differences. Following a similar approach to the definition of the wet and dry NWA summers, the strong and weak Mascarene highs are defined as the nine maximum years and nine minimum years based on the MHI. The strong Mascarene high years are 1950, 1962, 1973, 1981, 1993, 1996, 1997, 1998, and 1999, while the weak years are 1948, 1949, 1955, 1956, 1968, 1971, 1976, 1983, and 1984. The circulation pattern in Figure 4a is similar to that in Figure 2, indicating that variability in NWA summer rainfall is closely linked to variations in the Mascarene high; i.e., during the strong years, strengthened anticyclonic circulations are seen over the southern Indian Ocean. In response to the intensified anticyclone, southerlies to the southwest of NWA are enhanced, which suggests that the zonal shear of the meridional wind is strengthened. This may be further supported by the strong correlation (R = 0.57) between MHI and the zonal shear of the meridional wind index, suggesting that the Mascarene high could accelerate the cyclonic vorticity over NWA. This point is further supported

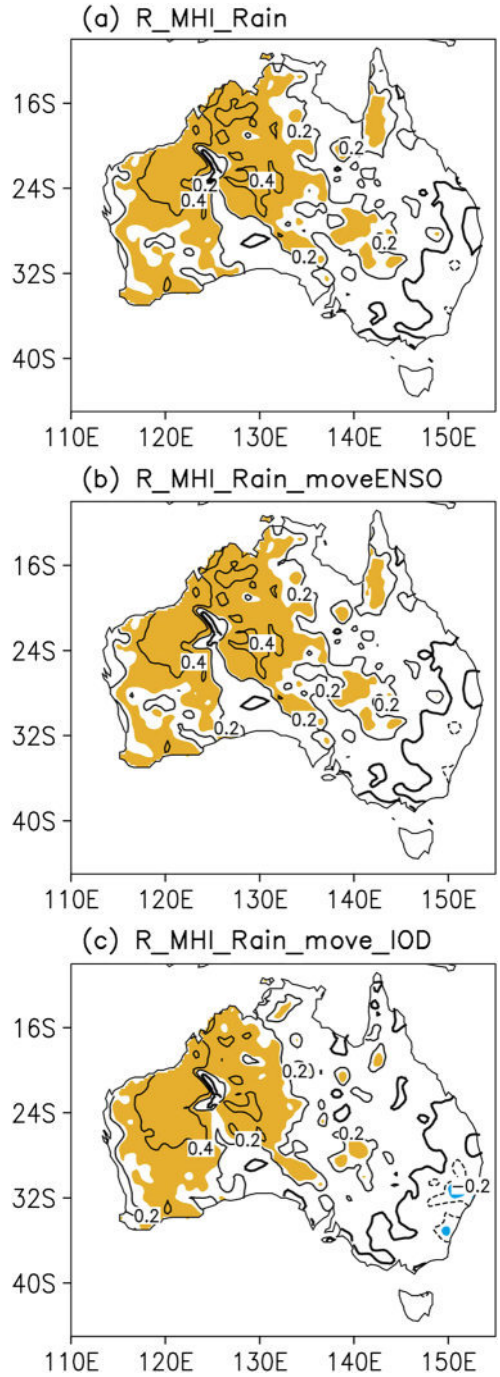

Figure 3. (a) Spatial distribution of correlation between the Mascarene high index (MHI) and Australian summer rainfall from 1948 to 2006. (b and c) As in Figure 3a, but for the partial correlation maps after removing the effects of the Niño 3.4 and IOD, respectively. Shading indicates significance at the 0.05 level.

by the significant correlation between the MHI and ALI (correlation coefficient of –0.43). In this sense, responding to the strengthened cyclonic circulation, anomalous northwesterlies are observed along the northwest boundary of NWA, transporting more moisture into NWA. This is further verified by the strong correlation between the MHI and moisture flux over the northwest boundary of NWA

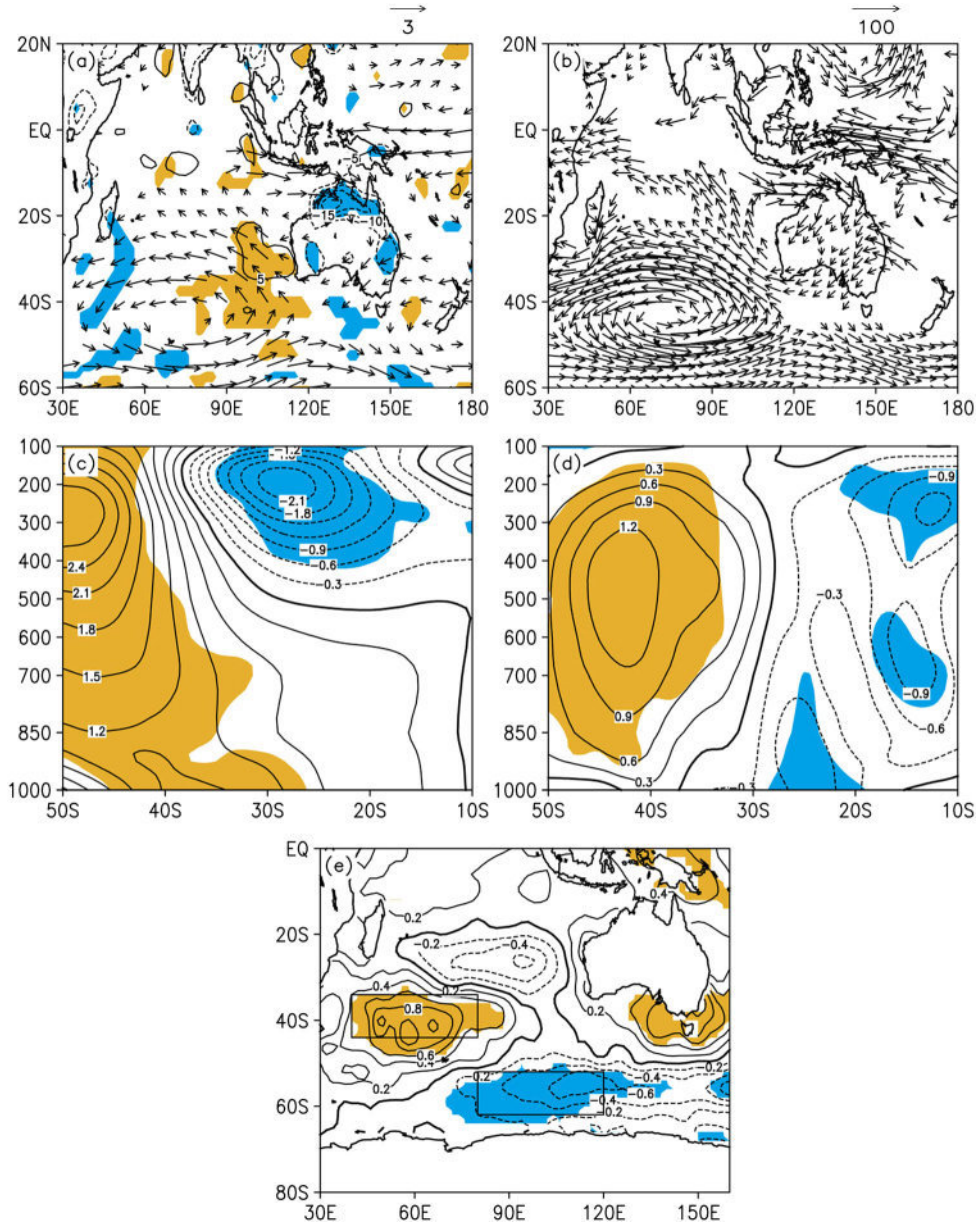

Figure 4. As in Figure 2, but for composite differences between years with a strong and weak Mascarene high. (a) Winds (vectors; m/s) at 850 hPa and divergence (contours; 10^{-6} s^{-1}) at 700 hPa. (b) Vertical integral moisture transport (g s^{-1} m^{-1} Pa^{-1}) and latitude-pressure sections for (c) Meridional wind (m/s) and (d) vertical velocity over 80°–130°E (Pa/s). (e) SST (°C). The SST gradient index within the southern Indian Ocean (SIOSGI) is defined as the normalized difference in area-averaged SST between the regions outlined by rectangles in Figure 4e. The strong Mascarene high years are 1950, 1962, 1973, 1981, 1993, 1996, 1997, 1998, and 1999, while the weak Mascarene high years are 1948, 1949, 1955, 1956, 1968, 1971, 1976, 1983, and 1984.

(R = 0.45), defined as the average integrated moisture flow between 1000 and 300 hPa across the hypotenuse in Figure 1a. This finding is evident in the distribution of the vertically integrated moisture transport (Figure 4b), consequently, anomalous convergence forms in the lower troposphere over NWA (Figure 4a), causing strengthened cyclonic vorticity. In terms of vertical velocity, pronounced negative anomalies occur over NWA, and positive anomalies occur over the southern Indian Ocean. Taking the vertical distribution of the meridional wind and vertical velocity together, an anomalous vertical circulation is seen with the ascending branch over NWA, and the subsidence branch over the region occupied by the Mascarene high. This suggests that both the Mascarene high and the Australian low are intensified during strong Mascarene high years.

[16] Figure 5 shows the standardized time series of NWA summer rainfall, ALI, MHI, and the moisture flux over the northwest boundary of NWA, revealing strong interdecadal and interannual variations over recent decades, with mostly positive polarities in the incoming moisture via the

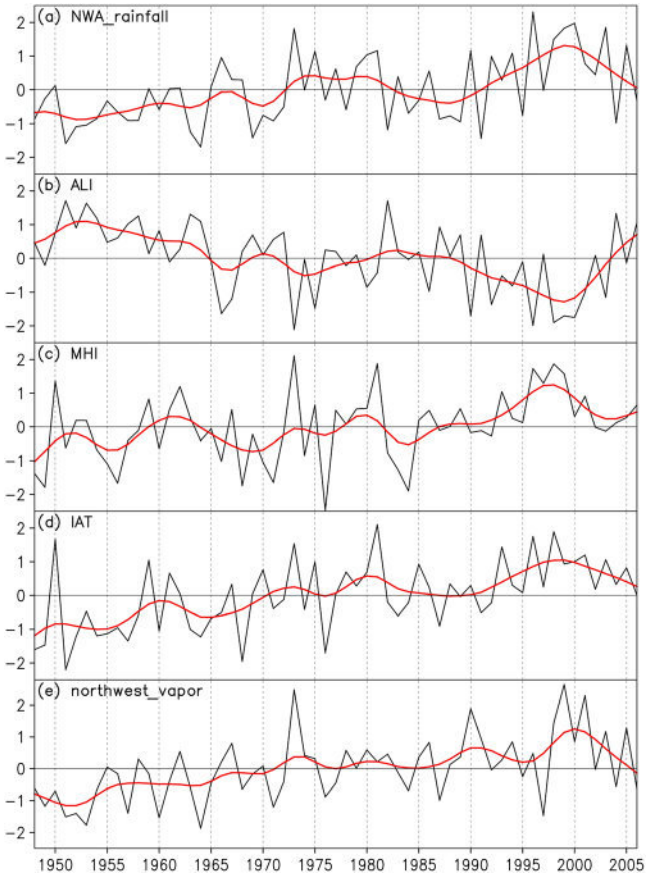

Figure 5. Normalized time series of (a) NWA summer rainfall, (b) Australian low index (ALI), (c) MHI, (d) the teleconnection wave train index from the southern Indian Ocean to northwest Australia (IAT), and (e) the ingoing moisture flux via the northwest boundary of NWA. The thick solid lines indicate 9 year Gaussian-type filtered values.

northwest boundary, NWA summer rainfall, and MHI since the 1990s. A suppressed Mascarene high is accompanied by a weak Australian low and less incoming moisture via the northwest boundary, which corresponds to less summer rainfall over NWA. During the past 20 years, the Mascarene high, Australian low, and incoming moisture have intensified, and summer rainfall over NWA has entered a positive phase. These relationships are highlighted by strong correlations among these factors, as mentioned above (see Table 1).

[17] Given this scenario, how does the Mascarene high transfer its influence onto NWA summer rainfall? To explore this issue, the correlation pattern between the MHI and vorticity in the upper troposphere is shown in Figure 6a. It is clear that a teleconnection wave train occurs from the southern Indian Ocean to NWA (IAT) with positive-negative-positive-negative centers located at around A, 80°E, 45°S; B, 90°E, 32.5°S; C, 115°E, 25°S; and D, 130°E, 15°S, respectively. This wave train is also evident in the cross section of the two successive correlation centers (Figure 6b). The wave train related to the Mascarene high is evident in the whole troposphere, particularly in the middle to upper levels of the troposphere. The linkage between the Mascarene high and IAT is further illustrated by the strong correlations between the teleconnection wave train index (defined as the sum of the MHI and vorticity correlation centers at 200 hPa, as shown in Figure 6a; i.e., IAT = A − B + C − D) and MHI, with a correlation coefficient of 0.74. This result suggests that the variations of the Mascarene high are associated with a teleconnection wave train, by which the signal is transported to NWA and thus influences the circulation above NWA. The significant negative correlations at 130°E, 15°S (within NWA), in both the upper and lower troposphere, imply that intensification of the Australian low and increased summer rainfall over NWA are favored when the Mascarene high is strong. This point is further established by the strong correlation between the area-averaged vorticity over 120°–150°E, 20°–10°S (marked by the rectangle in Figure 6a) over NWA at 200 hPa and the vorticity in the lower troposphere within NWA (Figure 6d). Positive correlations occur over NWA, while negative correlations occur over the region of the Mascarene high. This suggests that the variations in the Australian low are significantly connected to those in the upper troposphere vorticity (with a correlation coefficient of 0.51), in turn suggesting that the Mascarene high influences NWA summer rainfall via the teleconnection wave train. To demonstrate the approximate propagation direction of the wave train related to the Mascarene high, the spatial distribution of correlations between *Plumb*'s [1985] stationary wave activity flux (vectors), calculated from the anomalous stream function, and MHI is displayed in Figure 6c. We see a strong divergence in the scope of the anomalous Mascarene high, and it is clear that the wave train related to the Mascarene high propagates northeastward toward NWA, similar to the wave train in Figure 6a. Moreover, this wave train does not cross to northeast Australia, implying that northwest and northeast Australia are controlled by different circulation patterns, and thus exhibit opposite long-term rainfall trends as shown in Figure 1b. We even see that the westward propagation of the wave train related to the Mascarene high terminates to the west of 50°E, and the eastward propagation terminates to the west of 150°E, indicating that northward propagation is the only available direction for the Mascarene high–related wave trains to affect the climate of Australia. Our interpretation regarding the Rossby wave propagation is consistent with that indicated by *Davidson et al*. [2007], in which the Rossby wave propagation from the south Indian Ocean is also postulated as a mechanism for driving NWA summer rainfall; however, they focused on the synoptic scale and the influence on the onset of the Australian summer monsoon.

[18] Given the above observations, the strengthening of the Mascarene high over recent decades may reflect the fact that underlying forcing (e.g., SST) of the Mascarene high variability has intensified in recent years. To test this possibility, we analyzed composite differences between strong and weak Mascarene high years in terms of SST (Figure 4e). Pronounced positive SST anomalies to the northwest part of the anomalous Mascarene high, coupled with negative anomalies to the southeast, suggest an intensified SST gradient beneath the anomalous Mascarene high region over the southern Indian Ocean. Note that a similar anomalous SST pattern is observed in the Met Office Hadley Centre's sea ice and SST data sets [*Rayner et al*., 2003] (figure not shown), indicating the reliability of our findings. The anticyclonic circulation would be intensified under the influence of this

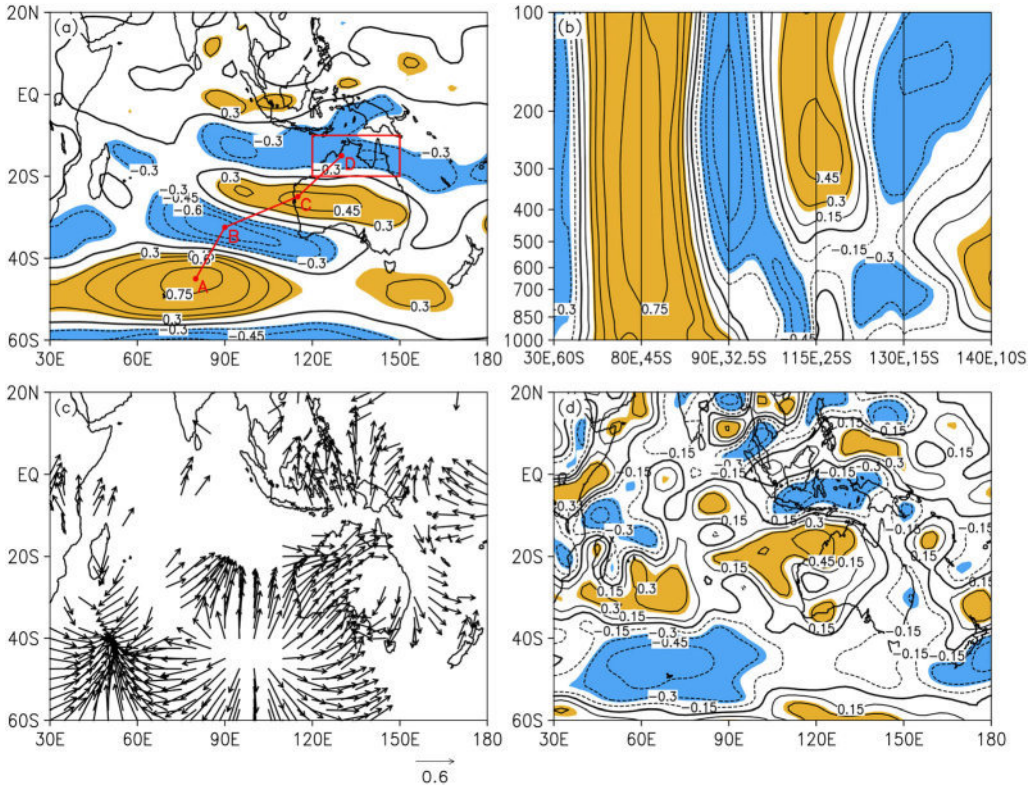

Figure 6. (a) The spatial correlation distribution between the MHI and vorticity at 200 hPa. (b) As in Figure 6a, but for the vertical section along the solid line labeled A (80°E, 45°S), B (90°E, 32.5°S), C (115°E, 25°S), and D (130°E, 15°S) in Figure 6a. (c) As in Figure 6a, but for the correlations with wave activity flux; only the vectors significant at the 0.05 level are given. (d) As in Figure 6a, but for the correlation between the area-averaged vorticity at 200 hPa over 120°–150°E, 20°–10°S as scaled in Figure 6a and the vorticity at 700 hPa. Shading indicates significance at the 0.05 level.

anomalous SST structure, as indicated by a significant positive correlation (R = 0.62) between MHI and the SST gradient index within the southern Indian Ocean (SIOSGI), defined as the difference in SST anomalies between the regions 40°–80°E, 44°–34°S and 80°–120°E, 62°–52°S. This suggests that the strength of the Mascarene high is closely linked to the SST gradient in the surrounding regions.

[19] The above analysis reveals that the Mascarene high has shown a pronounced intensification over recent decades, which has accelerated the cyclonic vorticity over NWA. In addition, the variation of the Mascarene high is associated with a teleconnection wave train, by which it propagates its influence from the southern Indian Ocean to NWA, and so strengthens the cyclonic vorticity over NWA. Both of these changes favor increased summer rainfall over NWA.

5. Physical Mechanisms of the Strengthened Mascarene High

[20] As noted above, variations in the SIOSG contribute to variability in the Mascarene high. As the ocean alone lacks a mechanism by which to produce the observed SST anomalies, the anomalies must be the result of coupled mechanisms [*Wu et al.*, 2009b]. In terms of the Southern Hemisphere at middle to high latitudes during summer, the dominant mode is the SAM, which has shown a significant upward trend over recent decades [e.g., *Marshall*, 2003; *Visbeck*, 2009; *Feng et al.*, 2010b]. In fact, *Wu et al.* [2009b] have already reported that the preceding boreal autumn (September–November) SAM has an important influence on the subsequent SSTs at middle latitudes. Given this result, we now investigate the influence of the SAM on the SIOSG.

[21] Figure 7a shows the lead-lag correlation between SAMI and SIOSGI. The significant relationship between SAMI and SIOSGI mainly exists when SAM leads SIOSG from the preceding October to the following February, suggesting the preceding variability of SAM has an important influence on the subsequent SIOSG. Their significant relationship starts in the preceding October, and persists to the following February, with the maximum values occurring when SAM leads SIOSG by about one month in November; a similar result is obtained using detrended data (figure not shown). This suggests that the spring and summer (October to February) SAM has a significant influence on the contemporaneous and ensuing SIOSG variation.

[22] To understand how the spring SAM affects SST variations, we first examined surface wind speed anomalies associated with the spring SAM. Figure 8 shows the lead-lag correlations between the latitudinally averaged surface wind speeds and spring SAMI. A significant correlation dipole begins during October, with positive correlations south of 50°S in the region of 80°–120°E, and negative correlations between 45°S and 30°S within 40°–80°E. The

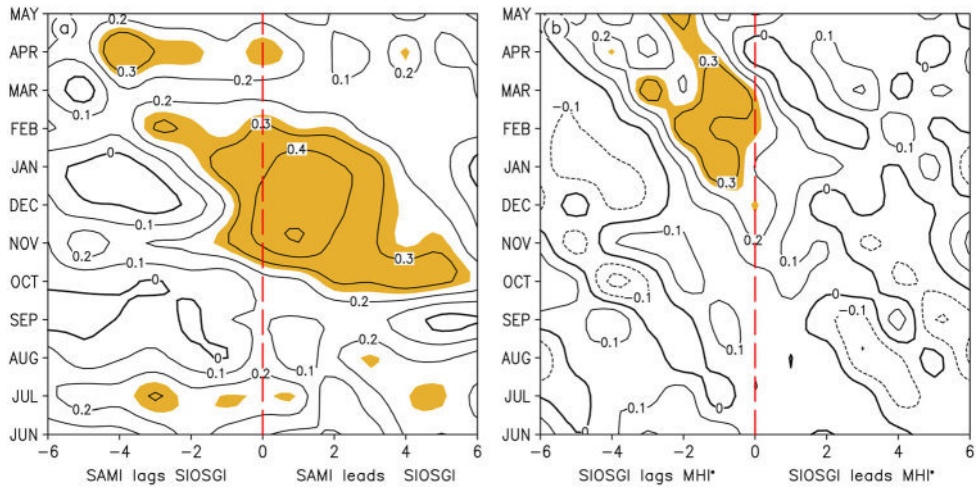

Figure 7. (a) Lead-lag correlation between SAMI and SIOSGI. (b) As in Figure 7a, but for the correlation between the component of the Mascarene high that is independent from SAM (MHI*) and SIOSGI. Shading indicates significance at the 0.05 level.

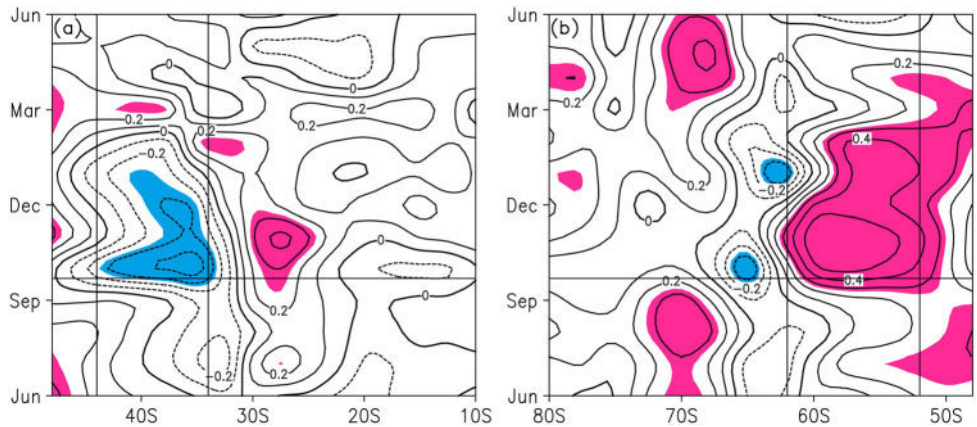

Figure 8. As in Figure 7, but for the lead-lag correlations between spring SAMI and zonal mean surface wind speed averaged over (a) 40°–80°E and (b) 80°–120°E.

positive correlation pole is sustained from October to March, while the negative correlation pole lasts for three months, becoming insignificant after December. This finding indicates that the wind speed at high latitudes within 80°–120°E is stronger than normal in strong spring SAM years, whereas winds at middle latitudes (i.e., 45°–30°S) within 40°–80°E are weaker than normal. As a strong sea surface wind speed often favors cold SST anomalies due to latent heat flux exchange, the dipole surface wind speed pattern is accompanied by a similar pattern in SST, with negative correlations at high latitudes and positive correlations at middle latitudes in the southern Indian Ocean (Figure 4e). In addition, because the positive correlations with surface wind speed at high latitudes are much stronger than those at middle latitudes, the associated SST anomalies at high latitudes are much more extensive than those at middle latitudes (Figure 4e). The correlation dipoles are maintained even if the linear trends are removed, suggesting a strong relationship between the spring SAM and the SIOSG (figures not shown).

[23] The above analysis indicates that the preceding spring and following summertime SST dipole pattern associated with variations in the Mascarene high can be attributed to the preceding spring SAM. In years with a strong spring SAM, wind speed is intensified at high latitudes within 80°–120°E, but reduced at middle latitudes within 40°–80°E. In response to the wind anomalies, negative SST anomalies occur at high latitudes, and positive SST anomalies occur at middle latitudes, corresponding to an enhanced thermal gradient within the southern Indian Ocean. Furthermore, the SIOSG shows strong persistence (figure not shown), since the correlation of SIOSGI between the preceding spring and following summer yields a correlation coefficient of 0.65, suggesting the SST itself possesses a strong autocorrelation, and that SST anomalies from the preceding spring may affect the subsequent SST distribution, thereby influencing the strength of the Mascarene high.

[24] These findings regarding the influences of the SIOSG on the strength of the Mascarene high are further illustrated by the evolution of circulation anomalies associated with the

SIOSG (Figure 9). Positive geopotential height anomalies are observed over the southern Indian Ocean in the larger SST gradient years as early as October–November when the SAM-SIOSG relationship is significant, and are accompanied by anticyclonic wind anomalies that correspond to an enhanced Mascarene high. In addition to the temporal evolution (from October–November to January–February), the circulation anomalies associated with the SIOSG become stronger, indicating the strengthening of the anomalous Mascarene high. Also, the anomalous circulation associated with the SIOSG during December–January and January–February is similar to that during anomalous Mascarene high years (Figure 4a). This result implies that variations in the SIOSG have an important influence on the variability of the Mascarene high. In addition, we see that the anomalous southerlies along the western coast of NWA strengthen along with the evolution from November to February, and that negative geopotential height anomalies, as well as cyclonic wind anomalies, are observed within NWA during December–January and January–February. However, no significant signal is seen during October–November or November–December. Similar anomalous patterns within NWA can also be observed in the spatial distribution of the correlation between the SIOSGI and the circulations (figures not shown). This implies that variations in the summer SIOSG have an influence over NWA by contributing to the circulation anomalies within the region, which encourages the formation of favorable rainfall circulation anomalies that are associated with the stronger Mascarene high years. This interpretation is further supported by the significant correlation between SIOSG and NWA summer rainfall (R = 0.38).

[25] These results indicate that the preceding SAM influences the variation of the SIOSG, which in turn contributes to the variability of the Mascarene high. However, as reported previously, the variations of the Mascarene high are closely linked to those of the SAM, and air-sea interaction in the extratropics is driven mainly from the air rather than from the ocean [e.g., *Davis*, 1976; *Wallace and Jiang*, 1987]. Thus, one noticeable issue regards whether the variations in the SIOSG are due to the Mascarene high rather than the SAM. To address this point, we divided the variations of the Mascarene high into two components as follows:

$$\mathrm{MHI} = \mathrm{RSAM} + \mathrm{MHI}^{*} \tag{1}$$

$$\mathrm{RSAM} = r \times \left[\frac{\sigma(\mathrm{MHI})}{\sigma(\mathrm{SAMI})}\right] \times \mathrm{SAMI} \tag{2}$$

$$\mathrm{MHI}^{*} = \mathrm{MHI} - r \times \left[\frac{\sigma(\mathrm{MHI})}{\sigma(\mathrm{SAMI})}\right] \times \mathrm{SAMI} \tag{3}$$

[26] Here RSAM is the variability of SAM related to the Mascarene high (represented by a linear fit of SAMI to

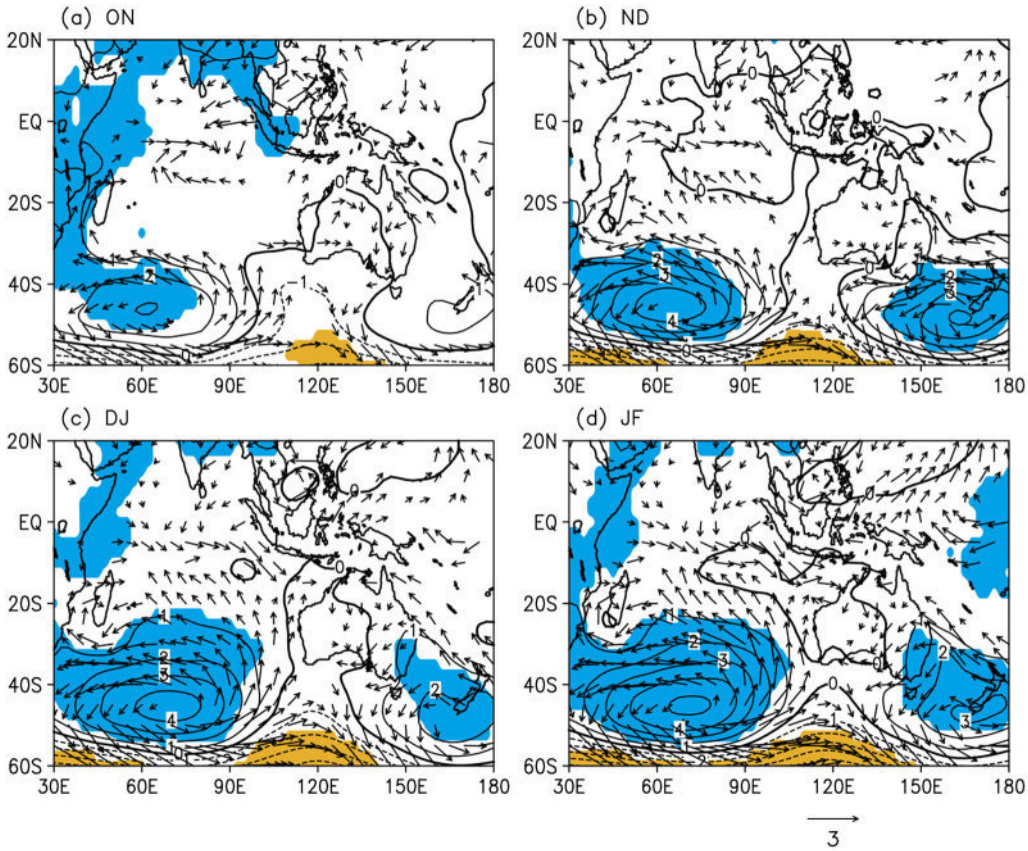

Figure 9. As in Figure 2, but for the composite differences of geopotential height and surface winds between years with a strong and weak SIOSGI during four successive periods: (a) October–November, (b) November–December, (c) December–January, and (d) January–February.

MHI), MHI* is the variability of the Mascarene high that is unrelated to SAM, r denotes the correlation coefficient between the MHI and SAMI, and σ(MHI) and σ(SAMI) are the standard deviations of MHI and SAMI, respectively. This method is identical to the semi–partial correlation method, and verifies whether the variability of the Mascarene high that is unrelated to the SAM is connected to the variations in SST. In this way, the lead-lag correlation between MHI* and SIOSGI can be explored as shown in Figure 7b. Similarly, the significant correlation between them mainly occurred when the SIOSG was lagged. However, this only occurs between January and March, when the SIOSG lags the Mascarene high for about 1–2 months, suggesting the linkage between the SIOSG and the Mascarene high in summer is mainly due to the variability of the SAM. That is, the variations in the SIOSG in summer are largely due to the variability of the preceding and simultaneous SAM.

[27] To add further support to the influence of the SIOSG on variations in the Mascarene high, we performed numerical experiments using the CAM3 model, which is able to reproduce the climate features as observed [e.g., *Wu et al.*, 2009b; *Li et al.*, 2012]. The control run was integrated for 15 years, and was used to derive a reference state. The sensitivity experiments were integrated for 17 years, with the latter 15 years used to construct a 15-member ensemble mean to reduce uncertainties arising from different initial conditions. To isolate and mimic the impact of SST variations on atmospheric circulation, we designed two sets of experiments, with the difference between the sensitivity experiments and control run being a 1 °C increase (decrease) and decrease (increase) in SST over the areas 40°–80°E, 44°–34°S and 80°–120°E, 62°–52°S during the preceding spring, and corresponding to the positive and negative phase of the SIOSG, respectively. The amplitude of SST variations in the sensitivity experiment was comparable to the SST anomalies associated with variations in the Mascarene high (Figure 4e), because the values of the anomalous center were beyond 1 °C at middle latitudes, and beyond –0.6 °C at high latitudes.

[28] Figure 10 shows the difference in circulation between the two sensitivity experiments and the control run during summertime. It is clear that the enhanced (suppressed) SIOSG excites positive (negative) geopotential height anomalies and strengthens (weakens) the anticyclonic circulation, which corresponds to an intensified (suppressed) Mascarene high. In addition, we see an anomalous negative (positive) geopotential height center over NWA, similar to that in Figures 9c and 9d. This finding supports the interpretation presented above, and further indicates that variations in the SIOSG contribute to variations in the Mascarene high.

[29] A further issue to be resolved is whether the SAM has a direct influence on NWA summer rainfall. To this end, the correlation patterns between the SAMI and summer rainfall are shown in Figure 11. It is clear that a relationship exists between the SAM and NWA summer rainfall (correlation coefficient of 0.39, significant at the 0.05 level); however, if the effect of the Mascarene high in the relationship between the SAM and rainfall is removed, we find that the significant correlation between the SAM and rainfall essentially disappears (Figure 11b). By contrast, the relationship between the Mascarene high and rainfall over NWA is still significant when the effect of the SAM is removed (Figure 11c). This point is further confirmed by the partial correlation coefficients among them (i.e., the partial correlation coefficient between the SAM and NWA summer rainfall, after removing the Mascarene high is 0.04, while it is 0.31 for the partial correlation between the Mascarene high and NWA summer rainfall when the effect of the SAM is removed). This result suggests the relationship between the Mascarene high and NWA summer rainfall is not a response to the SAM; instead, it is the Mascarene high that contributes to variations in NWA summer rainfall.

6. Conclusions and Discussion

[30] This study examined the causes of increasing rainfall over NWA, with a focus on extratropical factors. Since the middle of the 20th century, rainfall across Australia has shown contrasting long-term trends, decreasing over most areas, but increasing in NWA, and this represents a potential source of water for the drier regions. We found that the Mascarene high has an important influence on summer rainfall in NWA. The variations of the Mascarene high are connected to a teleconnection wave train from the southern Indian Ocean to NWA in the upper troposphere, by which

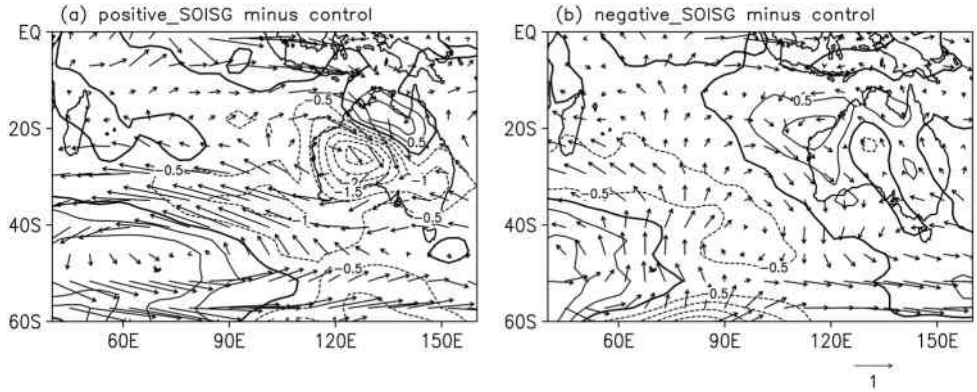

Figure 10. (a) Differences in wind (vectors; m/s) and geopotential height (contours; m) at 850 hPa between the simulated positive SIOSG phase and the control run. (b) As in Figure 10a, but for the differences between the simulated negative SIOSG phase and the control run.

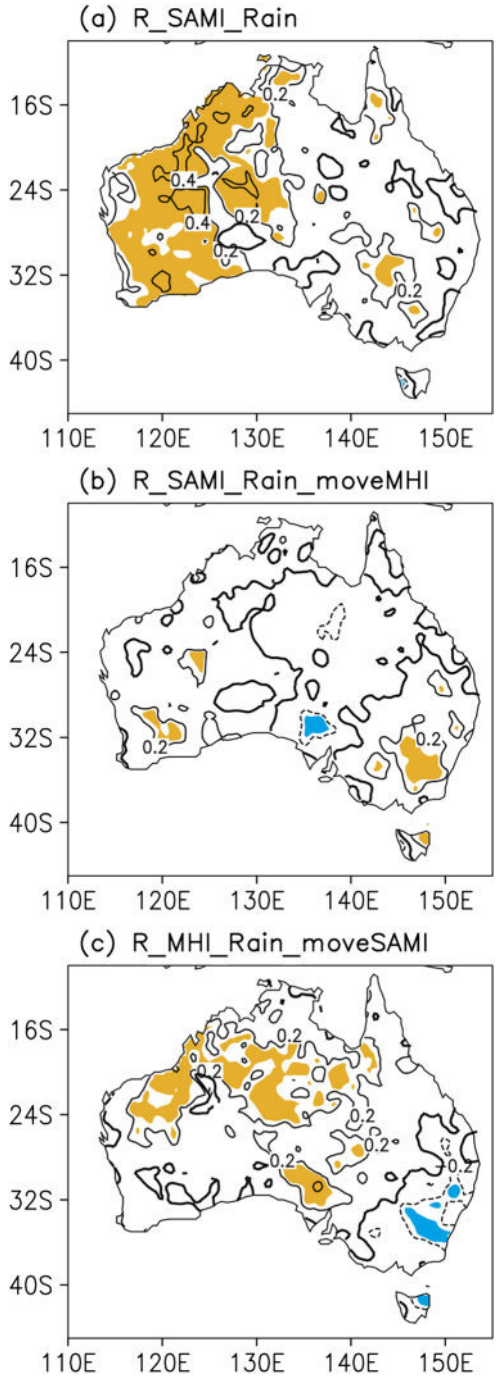

Figure 11. (a) As in Figure 3a, but for the correlation between the SAMI and Australian summer rainfall. (b) As in Figure 11a, but for the partial correlation between the SAMI and rainfall after removing the effect of MHI. (c) As in Figure 11a, but for the partial correlation between the MHI and rainfall after removing the effect of SAMI.

the signals are propagated to circulations over NWA, and thus influence NWA summer rainfall. Accordingly, strengthened cyclonic vorticity and northeastward moisture transport from midlatitudes are observed in the lower troposphere over NWA during strong Mascarene high years. At the same time, an anomalous vertical circulation forms with an ascending branch over NWA and a descending branch over the Mascarene high region. This causes summer rainfall over NWA to be enhanced. Moreover, the strength of the Mascarene high shows a clear upward trend over the past 6 decades, which is associated with increased NWA summer rainfall.

[31] The SAM of the preceding spring shows potential to predict the strength of the Mascarene high via SST. The SST gradient within the southern Indian Ocean would be strengthened in both the preceding spring and concurrent summer when the preceding spring SAM has a strong polarity, resulting in intensified anticyclonic circulation and an enhanced Mascarene high. On the other hand, we found that the wave train related to the Mascarene high was not significant when a similar analysis was performed with the SIOSG or SAM, but with the effects of the Mascarene high removed. In contrast, the Mascarene high–related wave train was still significant, but weakened, when the effects of the SIOSG and SAM were removed (Figure 12). This result supports the conclusion that the wave train is more closely connected to the variations of the Mascarene high, and suggests that both the influences from the SIOSG and SAM on the teleconnection wave train are via the Mascarene high. However, as variations of the SAM and SIOSG contribute to variations of the Mascarene high, this implies that the Mascarene high may act as a bridge between the SIOSG and the wave train.

[32] The increasing signal of NWA summer rainfall is mainly an interdecadal variability (Figure 5a) that is the opposite of the parallel variations in northeast Australia's summer rainfall. This observation may indicate that the dipole pattern in summer rainfall variability over northern Australia reflects interdecadal variations, and rainfall over these two regions may be controlled by different climatic factors. This study has shed some light on this issue, and we have demonstrated that wave train activity associated with the Mascarene high could not propagate to northeast Australia (Figure 6c), and also raised the possibility that climatic factors from the subtropics contribute to the summer rainfall of NWA. However, *Li et al.* [2012] point out that rainfall variations over northeast Australia are associated with tropical factors (i.e., the TASM). Moreover, circulation over NWA shows barotropic features (Figure 6b), which are unlike those of northeast Australia [e.g., *Li et al.*, 2012]. These points provide some insight into the contrasting rainfall variability over NWA and northeast Australia. A more detailed study of the similarities and differences between the rainfall and circulation features over NWA and northeast Australia is required. In addition, the East Asian winter monsoon (EAWM) has shown strong interdecadal variations over recent decades [e.g., *Wu and Zhang*, 2006; *Zhou et al.*, 2007a, 2009; *Li et al.*, 2011a], and it appears that the ENSO has a significant impact on the EAWM [*Zhou et al.*, 2007a, 2007b; *Li et al.*, 2010, 2011b]. Consequently, it may be interesting to investigate whether this variation contributes to the variability of NWA summer rainfall, and the relationships among the ENSO, EAWM, and NWA summer rainfall, considering the impact of ENSO on the NWA summer rainfall is limited [*Li et al.*, 2012], whereas play important role in influencing the EAWM. These issues are left as open questions that require further investigation.

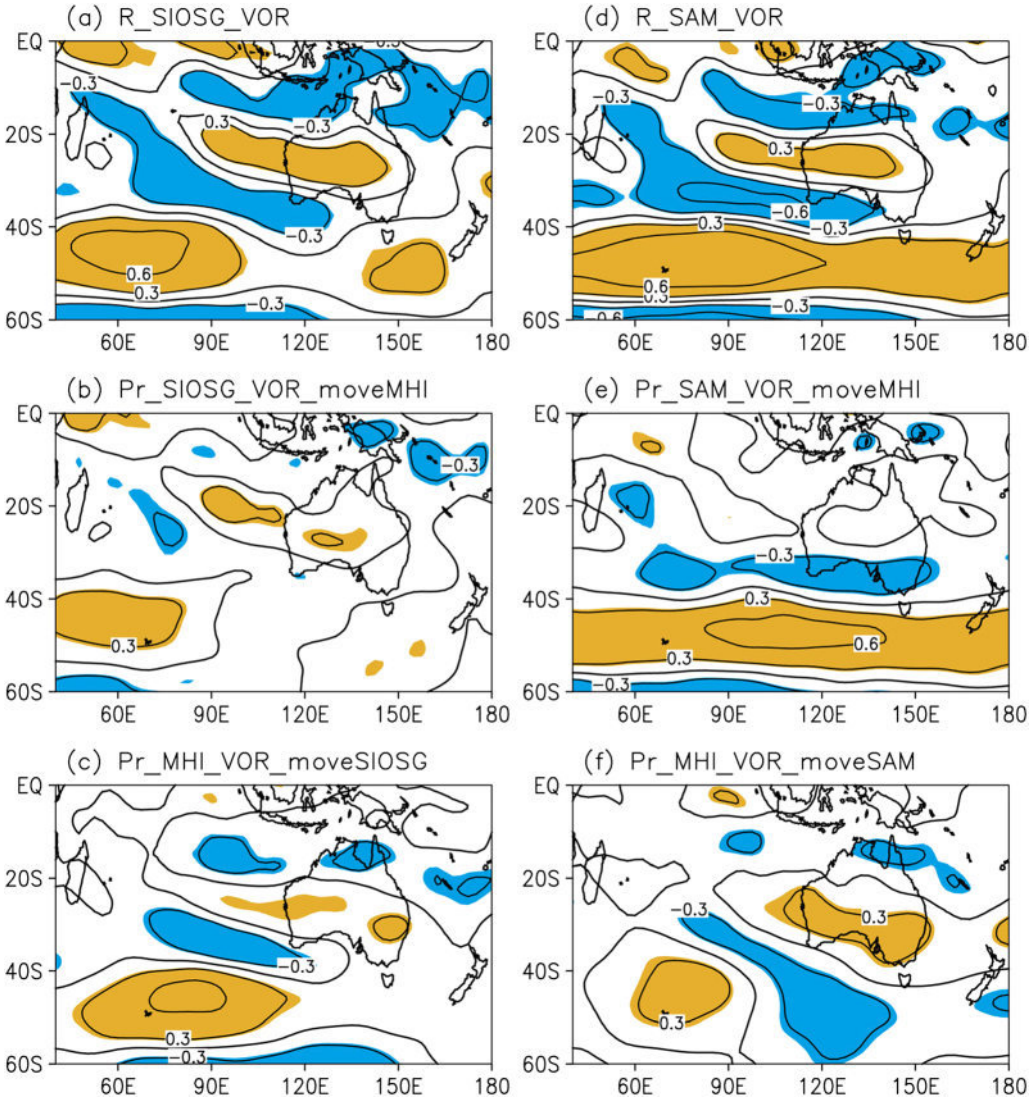

Figure 12. (a) As in Figure 6a, but for the correlation between the SIOSG and vorticity at 200 hPa. (b) As in Figure 12a, but for the partial correlation after removing the effects of the Mascarene high. (c) Correlation between the MHI and vorticity after removing the effects of the SIOSG. (d) As in Figure 12a, but for the correlation between the SAMI and vorticity. (e) As in Figure 12d, but for the partial correlation after removing the effects of the Mascarene high. (f) Correlation between the MHI and vorticity after removing the effects of the SAM.

[33] **Acknowledgments.** This work was jointly supported by the 973 Program (2010CB950400) and the National Natural Science Foundation of China (41030961, 41205046).

References

Ashok, K., Z. Y. Guan, and T. Yamagata (2003), Influence of the Indian Ocean dipole on the Australian winter rainfall, *Geophys. Res. Lett.*, *30*(15), 1821, doi:10.1029/2003GL017926.

Ashok, K., S. K. Behera, S. A. Rao, H. Weng, and T. Yamagata (2007), El Niño Modoki and its teleconnection, *J. Geophys. Res.*, *112*, C11007, doi:10.1029/2006JC003798.

Berry, G., M. J. Reeder, and C. Jakob (2011), Physical mechanisms regulating summertime rainfall over northwestern Australia, *J. Clim.*, *24*, 3705–3171.

Collins, W. D., et al. (2006), The formulation and atmospheric simulation of the Community Atmosphere Model version 3 (CAM3), *J. Clim.*, *19*, 2144–2161.

Davis, R. E. (1976), Predictability of sea surface temperature and sea level pressure anomalies over the North Pacific Ocean, *J. Phys. Oceanogr.*, *6*, 249–266.

Drosdowsky, W. (1993), An analysis of Australian seasonal rainfall anomalies: 1950–1987. II: Temporal variability and teleconnection patterns, *Int. J. Climatol.*, *13*, 111–149.

Drosdowsky, W., and M. Williams (1991), The Southern Oscillation in the Australian region. Part I: Anomalies at the extremes of the oscillation, *J. Clim.*, *4*, 619–638.

Davidson, N. E., K. Tory, M. J. Reeder, and W. L. Drosdowsky (2007), Extratropical-tropical interaction during onset of the Australian monsoon: Reanalysis diagnostics and idealized dry simulations, *J. Atmos. Sci.*, *64*, 3475–3498.

England, M. H., C. C. Ummenhofer, and A. Santoso (2006), Interannual rainfall extremes over southwest Western Australia linked to Indian Ocean climate variability, *J. Clim.*, *19*, 1948–1969.

Feng, J., and J. P. Li (2011), Influence of El Niño Modoki on spring rainfall over South China, *J. Geophys. Res.*, *116*, D13102, doi:10.1029/2010JD015160.

Feng, J., J. P. Li, and Y. Li (2010a), A monsoon-like southwest Australian circulation and its relation with rainfall in southwest Western Australia, *J. Clim.*, *23*, 1334–1653.

Feng, J., J. P. Li, and Y. Li (2010b), Is there a relationship between the SAM and southwest Western Australian winter rainfall?, *J. Clim.*, *23*, 6082–6089.

Grose, W. L., and B. J. Hoskins (1979), On the influence of orography on large-scale atmospheric flow, *J. Atmos. Sci.*, *36*, 223–234.
Hendon, H. H., D. W. Thompson, and M. C. Wheeler (2007), Australian rainfall and surface temperature variations associated with the Southern Hemisphere annular mode, *J. Clim.*, *20*, 2452–2467.
Hsu, H. H., and S. H. Lin (1992), Global teleconnections in the 250-mb stream function field during the Northern Hemisphere winter, *Mon. Weather Rev.*, *120*, 1169–1190.
Hung, C., and M. Yanai (2004), Factors contributing to the onset of the Australian summer monsoon, *Q. J. R. Meteorol. Soc.*, *130*, 739–758.
Indian Ocean Climate Initiative (2002), Climate variability and change in southwest Western Australia, technical report, 34 pp., Indian Ocean Clim. Initiative Panel, Perth, West. Aust., Australia.
Jones, D. A., and G. Weymouth (1997), An Australian monthly rainfall dataset, *Tech. Rep. 70*, 19 pp., Bur. of Meteorol., Melbourne, Victoria, Australia.
Kalnay, E., et al. (1996), The NCEP/NCAR 40-year reanalysis project, *Bull. Am. Meteorol. Soc.*, *77*, 437–471.
Li, J. P., Z. W. Wu, Z. H. Jiang, and J. H. He (2010), Can global warming strengthen the East Asian summer monsoon?, *J. Clim.*, *23*, 6696–6705.
Li, J. P., G. X. Wu, and D. X. Hu (2011a), Ocean-Atmosphere Interaction Over the Joining Area of Asia and Indian-Pacific Ocean and Its Impact on the Short-Term Climate Variation in China, vol. *1*, China Meteorol. Press, Beijing.
Li, J. P., G. X. Wu, and D. X. Hu (2011b), Ocean-Atmosphere Interaction Over the Joining Area of Asia and Indian-Pacific Ocean and Its Impact on the Short-Term Climate Variation in China, vol. *2*, China Meteorological Press, Beijing.
Li, J. P., J. Feng, and Y. Li (2012), A possible cause of decreasing summer rainfall in northeast Australia, *Int. J. Climatol.*, *32*(7), 995–1005, doi:10.1002/joc.2328.
Li, Y., W. J. Cai, and E. P. Campbell (2005), Statistical modeling of extreme rainfall in southwest Western Australia, *J. Clim.*, *18*, 852–863.
Lin, Z. D., and Y. Li (2012), Remote influence of the tropical Atlantic on the variability and trend in northwest Australia summer rainfall, *J. Clim.*, *25*, 2408–2420.
Marshall, G. J. (2003), Trends in the southern annular mode from observations and reanalyses, *J. Clim.*, *16*, 4134–4143.
McBride, J. L., and N. Nicholls (1983), Seasonal relationships between Australian rainfall and the Southern Oscillation, *Mon. Weather Rev.*, *111*, 1998–2004.
Murphy, B. F., and J. Ribbe (2004), Variability of southeastern Queensland rainfall and climate indices, *Int. J. Climatol.*, *24*, 703–721.
Nan, S. L., and J. P. Li (2003), The relationship between summer precipitation in the Yangtze River valley and the boreal spring Southern Hemisphere annular mode, *Geophys. Res. Lett.*, *30*(4), 2266, doi:10.1029/2003GL018381.
Nicholls, N., B. Lavery, C. Frederiksen, W. Drosdowsky, and S. Torok (1996), Recent apparent changes in relationships between the El Niño–Southern Oscillation and Australian rainfall and temperature, *Geophys. Res. Lett.*, *23*, 3357–3360.
Plumb, R. A. (1985), On the three-dimensional propagation of stationary waves, *J. Atmos. Sci.*, *42*, 217–229.
Rayner, N. A., D. E. Parker, E. B. Horton, C. K. Folland, L. V. Alexander, D. P. Rowell, E. C. Kent, and A. Kaplan (2003), Global analyses of sea surface temperature, sea ice, and night marine air temperature since the late nineteenth century, *J. Geophys. Res.*, *108*(D14), 4407, doi:10.1029/2002JD002670.
Rotstayn, L. D., et al. (2007), Have Australian rainfall and cloudiness increased due to the remote effects of Asian anthropogenic aerosols?, *J. Geophys. Res.*, *112*, D09202, doi:10.1029/2006JD007712.
Saji, N., et al. (1999), A dipole mode in the tropical Indian Ocean, *Nature*, *401*, 360–363.
Shi, G., et al. (2008), Variability and trend over the northwest Western Australian rainfall: Observations and coupled climate modeling, *J. Clim.*, *21*, 2938–2959.
Smith, I. (2004), An assessment of recent trends in Australia rainfall, *Aust. Meteorol. Mag.*, *53*, 163–173.
Smith, I., et al. (2000), Southwest Western Australian winter rainfall and its association with Indian Ocean climate variability, *Int. J. Climatol.*, *20*, 1913–1930.
Smith, T. M., and R. W. Reynolds (2004), Improved extended reconstruction of SST (1854–1997), *J. Clim.*, *17*, 2466–2477.
Taschetto, A. S., and M. H. England (2008), An analysis of late 20th century trends in Australian rainfall, *Int. J. Climatol.*, *29*(6), 791–807.
Taschetto, A. S., and M. H. England (2009), El Niño Modoki impacts on Australian rainfall, *J. Clim.*, *22*, 3167–3174.
Terray, P., S. Dominiak, and P. Delecluse (2005), Role of the southern Indian Ocean in the transitions of the monsoon-ENSO system during recent decades, *Clim. Dyn.*, *24*, 169–195.
Thompson, D. W., and D. J. Lorenz (2004), The signature of the annular modes in the tropical troposphere, *J. Clim.*, *17*, 4330–4342.
Thompson, D. W., and J. M. Wallace (2000), Annular modes in the extratropical circulation. Part I: Month-to-month variability, *J. Clim.*, *13*, 1000–1016.
Visbeck, M. (2009), A station-based southern annular mode index from 1884 to 2005, *J. Clim.*, *22*, 940–950.
Wallace, J. M., and Q. R. Jiang (1987), On the observed structure of the interannual variability of the atmosphere/ocean climate system: Atmospheric and oceanic variability, *Q. J. R. Meteorol. Soc.*, *113*, 17–43.
Wang, G. M., and H. H. Hendon (2007), Sensitivity of Australian rainfall to inter-El Niño variations, *J. Clim.*, *20*, 4211–4226.
Wardle, R., and I. N. Smith (2004), Modeled response of the Australian monsoon to changes in land surface temperatures, *Geophys. Res. Lett.*, *31*, L16205, doi:10.1029/2004GL020157.
Weng, H. Y., et al. (2007), Impacts of recent El Niño Modoki on dry/wet conditions in the Pacific Rim during boreal summer, *Clim. Dyn.*, *29*, 123–129.
Weng, H. Y., S. K. Behera, and T. Yamagata (2009), Anomalous winter climate conditions in the Pacific Rim during recent El Niño Modoki and El Niño events, *Clim. Dyn.*, *32*, 663–674.
Wheeler, M. C. (2008), Seasonal climate summary Southern Hemisphere (summer 2007–08), mature La Niña, an active MJO, strongly positive SAM, and highly anomalous sea-ice, *Aust. Meteorol. Mag.*, *57*, 379–393.
Wu, B. Y., and R. H. Zhang (2006), Distinct modes of the East Asian winter monsoon, *J. Clim.*, *134*, 2165–2179.
Wu, Z. W., B. Wang, J. P. Li, and F. F. Jin (2009a), An empirical seasonal prediction model of the East Asian summer monsoon using ENSO and NAO, *J. Geophys. Res.*, *114*, D18120, doi:10.1029/2009JD011733.
Wu, Z. W., J. P. Li, B. Wang, and X. H. Liu (2009b), Can the Southern Hemisphere annular mode affect China winter monsoon? *J. Geophys. Res.*, *114*, D11107, doi:10.1029/2008JD011501.
Wu, Z. W., J. P. Li, Z. H. Jiang, J. H. He, and X. Zhu (2012), Possible effects of the North Atlantic Oscillation on the strengthening relationship between the East Asian summer monsoon and ENSO, *Int. J. Climatol.*, *32*, 794–800, doi:10.1002/joc. 2309.
Yoo, S. H., S. Yang, and C. Ho (2006), Variability of the Indian Ocean SST and its climate impact, *J. Geophys. Res.*, *111*, D03108, doi:10. 1029/2005JD006001.
Zhang, W. J., F. F. Jin, J. Li, and H. L. Ren (2011), Contrasting impacts of two-types El Niño over the western North Pacific during boreal autumn, *J. Meteorol. Soc. Jpn.*, *89*(5), 563–569.
Zheng, F., and J. P. Li (2012), Impact of preceding boreal winter southern annular mode on spring precipitation over south China and related mechanism [in Chinese], *Chin. J. Geophys.*, *55*(11), 3542–3557.
Zhou, W., et al. (2007a), Interdecadal variability of the relationship between the East Asian winter monsoon and ENSO, *Meteorol. Atmos. Phys.*, *98*, 283–293.
Zhou, W., C. Y. Li, and X. Wang (2007b), Possible connection between Pacific oceanic interdecadal pathway and East Asian winter monsoon, *Geophys. Res. Lett.*, *34*, L01701, doi:10.1029/2006GL027809.
Zhou, W., et al. (2009), Synoptic-scale controls of persistent low temperature and icy weather over Southern china in January 2008, *Mon. Weather Rev.*, *137*, 3978–3991.